Design of a Self-Tuning PI Controller for a STATCOM Using Particle Swarm Optimization

Chien-Hung Liu and Yuan-Yih Hsu, *Senior Member, IEEE*

***Abstract*—A self-tuning proportional-integral (PI) controller in which the controller gains are adapted using the particle swarm optimization (PSO) technique is proposed for a static synchronous compensator (STATCOM). An efficient formula for the estimation of system load impedance using real-time measurements is derived. Based on the estimated system load, a PSO algorithm, which takes the best particle gains, the best global gains, and previous change of gains into account, is employed to reach the desired controller gains. To demonstrate the effectiveness of the proposed PSO self-tuning PI controller for a STATCOM, experimental results for a system under different loading conditions are presented. Results from the self-tuning PI controller are compared with those from the fixed-gain PI controllers.**

***Index Terms*—Particle swarm optimization (PSO), reactive power compensation, self-tuning proportional-integral (PI) controller, static synchronous compensator (STATCOM), voltage regulation.**

I. Introduction

SIGNIFICANT voltage fluctuation at a load bus may be observed when there is a fault in the utility or a change in load, particularly when the load is a supplied power from the utility through a long distribution feeder. To improve the load voltage profile or the power factor, reactive power compensating devices such as shunt capacitors or static VAR compensators comprising a thyristor-controlled reactor and a fixed capacitor have been widely used in the industry [1], [2].

With the development of high-power semiconductor switches such as gate-turn-off thyristors and insulated-gate bipolar transistors, switch converter-type reactive power compensators, which are normally referred to as the static synchronous compensators (STATCOM), have been proposed in recent years [3]–[24]. Through high-frequency switching of the semiconductor switches, it has been found that voltage regulation and power factor correction can be achieved in a more efficient manner. Either voltage source inverter (VSI) [3]–[8], [17]–[19] or current source inverter [18]–[20] can be used to modulate the reactive power output of the STATCOM. In this paper, a STATCOM with VSI is employed to generate or absorb the required reactive power such that the load bus voltage can be regulated rapidly and effectively.

In the literature, decoupled control of d- and q-axis currents and voltages has been proposed to regulate the dc capacitor voltage and the ac system (load) voltage, respectively, in STATCOM controller design [5]–[8]. Proportional-integral (PI) controllers have been designed for the ac system voltage regulator, the dc voltage regulator, and the current regulators. Satisfactory dynamic responses have been reported for the STATCOM with PI controllers.

In the fixed-gain PI controller [5]–[8], the controller gains for the STATCOM were usually designed based on a linearized system equation for the system under a nominal load condition [5]–[8]. These controller gains remained fixed in daily operation of the STATCOM. Since system load changes with time in daily operation of the STATCOM, the system matrix, the closed-loop eigenvalues, and the dynamic performance will change. Therefore, to maintain good dynamic responses at all possible loading conditions, the controller gains need to be adapted based on system loading conditions. Artificial neural networks (ANNs) and fuzzy logic have been proposed to adapt the controller gains of the STATCOM [9], [11], [12], [25].

In this paper, a self-tuning PI controller using the particle swarm optimization (PSO) algorithm [26]–[28] is designed to adapt the controller gains for the STATCOM such that good dynamic responses can be achieved at all possible loading conditions. To maintain a constant voltage profile under disturbance conditions, the STATCOM must respond quickly (normally in a few cycles) following a disturbance. Thus, the controller gains must be reached in a very short period (e.g., in less than one cycle) by the self-tuning controller. PSO is employed in this paper to determine the required controller gains since it converges to a satisfactory solution in a very efficient manner. Several successful applications of the PSO have been reported in the literature [29]–[35].

The main advantages and the disadvantages of the conventional PI controller, the proposed PSO self-tuning controller, ANN controller, and fuzzy controller for the STATCOM are summarized in Table I. It is observed from Table I that the proposed self-tuning controller differs from the ANN approach in that it does not require offline training which is usually rather time-consuming. In addition, the PSO method does not require inference rules which are essential for fuzzy approaches [36]. However, the PSO method needs evaluation function in real-time applications.

Manuscript received December 2, 2008; revised July 8, 2009. First published August 7, 2009; current version published January 13, 2010. This work was supported by the National Science Council of the Republic of China under Contract 96-2221-E-002-187.

The authors are with the Department of Electrical Engineering, National Taiwan University, Taipei 106, Taiwan (e-mail: d93921009@ntu.edu.tw; yyhsu@cc.ee.ntu.edu.tw).

Digital Object Identifier 10.1109/TIE.2009.2028350

TABLE I
ADVANTAGES AND DISADVANTAGES OF CONTROL ALGORITHM

Algorithm	Operating Point Dependent	Needs Training	Needs Rule Base	Needs Evaluation Function	Ref.
PI	Yes	No	No	No	[7],[8]
ANN	No	Yes	No	No	[9],[11]
FUZZY	No	No	Yes	No	[12],[38],[39]
PSO	No	No	No	Yes	[26]-[35]

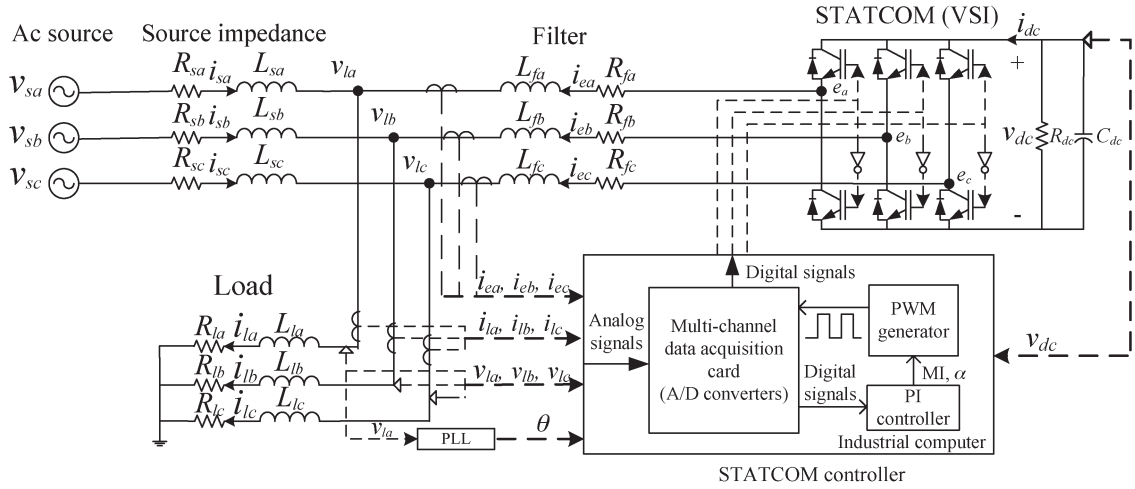

Fig. 1. Configuration of the system with a STATCOM.

The contents of this paper are as follows. First, the configuration of the system with a STATCOM is described. The dynamic equations for the load, the VSI ac-side system, and the VSI dc-side system are then derived. When the dynamic equations for the system are linearized around a nominal loading condition, we can proceed to design a fixed-gain PI controller for the STATCOM using the linearized state equations. Then, a self-tuning PI controller for the STATCOM is designed using the PSO method. Finally, experimental results are presented to demonstrate the effectiveness of the proposed PSO self-tuning PI controller for the STATCOM.

II. SYSTEM MODEL

As shown in Fig. 1, a three-phase load with load impedances $R_{la}+j\omega L_{la}$, $R_{lb}+j\omega L_{lb}$, and $R_{lc}+j\omega L_{lc}$ is a supplied power from a three-phase ac source with source voltages v_{sa}, v_{sb}, and v_{sc} and source impedances $R_{sa}+j\omega L_{sa}$, $R_{sb}+j\omega L_{sb}$, and $R_{sc}+j\omega L_{sc}$. To regulate load bus voltage v_l, a STATCOM comprising a VSI and a dc capacitor $C_{\rm dc}$ is connected to the system through a filter with impedances $R_{fa}+j\omega L_{fa}$, $R_{fb}+j\omega L_{fb}$, and $R_{fc}+j\omega L_{fc}$. Note that a resistance $R_{\rm dc}$ is used in Fig. 1 to cover the converter losses.

The output voltages for the VSI, e_a, e_b, and e_c, are controlled by the pulsewidth modulation (PWM) switching scheme in which the magnitudes and phase angles of the inverter output voltages are related to the modulation index (MI) and phase angle α of the control signal [5]–[7]. As shown in Fig. 1, the STATCOM controller comprises a multichannel data acquisition card, a PI controller, and a PWM generator. Note that the major functions of the multichannel data acquisition card include analog-to-digital converters, digital-to-analog converters, 16 digital I/O channels, 16 analog I/O channels, timers, counters, etc. To determine proper values for MI and α, the load voltages (v_{la}, v_{lb}, and v_{lc}), the load currents (i_{la}, i_{lb}, and i_{lc}), and the inverter currents (i_{ea}, i_{eb}, and i_{ec}) are fetched by the A/D converter at a sampling period of 1/15360 s (256 samples per cycle for a 60-Hz system). In addition, the phase angle for v_{la}, i.e., θ, is fetched through a phase-lock loop (PLL). These analog signals are converted to digital signals by the A/D converter before they are sent to the digital computer where a PI controller is designed to generate the required control variables MI and α. A PWM generator is built to generate the required switching pulses for the six switches in the VSI.

To determine proper gains for the PI controller, the dynamic equations for the system must be established first.

A. Load Model

As shown in Fig. 1, the three-phase load voltages in $a-b-c$ coordinates can be written as

$$\begin{bmatrix} v_{la} \\ v_{lb} \\ v_{lc} \end{bmatrix} = R_l \begin{bmatrix} i_{la} \\ i_{lb} \\ i_{lc} \end{bmatrix} + L_l \frac{d}{dt} \begin{bmatrix} i_{la} \\ i_{lb} \\ i_{lc} \end{bmatrix} \tag{1}$$

where balanced three-phase loads are assumed ($R_{la}=R_{lb}=R_{lc}=R_l$ and $L_{la}=L_{lb}=L_{lc}=L_l$). By using the well-known Park transformation [5]

$$T = \frac{2}{3} \begin{bmatrix} \cos\theta & \cos\left(\theta-\frac{2\pi}{3}\right) & \cos\left(\theta+\frac{2\pi}{3}\right) \\ -\sin\theta & -\sin\left(\theta-\frac{2\pi}{3}\right) & -\sin\left(\theta+\frac{2\pi}{3}\right) \\ \frac{1}{2} & \frac{1}{2} & \frac{1}{2} \end{bmatrix}. \tag{2}$$

Equation (1) can be transformed to the synchronously rotating reference frame as follows:

$$\begin{bmatrix} v_{ld} \\ v_{lq} \end{bmatrix} = R_l \begin{bmatrix} i_{ld} \\ i_{lq} \end{bmatrix} + L_l \frac{d}{dt} \begin{bmatrix} i_{ld} \\ i_{lq} \end{bmatrix} + L_l \begin{bmatrix} 0 & -\omega \\ \omega & 0 \end{bmatrix} \begin{bmatrix} i_{ld} \\ i_{lq} \end{bmatrix}. \quad (3)$$

Note that $\theta = \tan^{-1}(v_{lq}/v_{ld})$ [5] and v_{l0} is neglected in (3) since the system is assumed to be balanced. Since the angle θ is calibrated by the PLL at each cycle, the error will not be accumulated.

When i_l is replaced by the sum of the source current i_s and inverter current i_e, we have

$$\begin{bmatrix} v_{ld} \\ v_{lq} \end{bmatrix} = R_l \begin{bmatrix} i_{sd} \\ i_{sq} \end{bmatrix} + R_l \begin{bmatrix} i_{ed} \\ i_{eq} \end{bmatrix} + L_l \frac{d}{dt} \begin{bmatrix} i_{sd} \\ i_{sq} \end{bmatrix} + L_l \frac{d}{dt} \begin{bmatrix} i_{ed} \\ i_{eq} \end{bmatrix} + L_l \begin{bmatrix} 0 & -\omega \\ \omega & 0 \end{bmatrix} \begin{bmatrix} i_{sd} \\ i_{sq} \end{bmatrix} + L_l \begin{bmatrix} 0 & -\omega \\ \omega & 0 \end{bmatrix} \begin{bmatrix} i_{ed} \\ i_{eq} \end{bmatrix}. \quad (4)$$

B. VSI AC-Side Model

When the load current i_l in Fig. 1 is replaced by $i_s + i_e$, the source voltage v_s and inverter output voltage e can be written as

$$\begin{bmatrix} V_{sa} \\ V_{sb} \\ V_{sc} \end{bmatrix} = \frac{a_1}{L_l} \begin{bmatrix} i_{sa} \\ i_{sb} \\ i_{sc} \end{bmatrix} + \frac{b_1}{L_l} \frac{d}{dt} \begin{bmatrix} i_{ea} \\ i_{eb} \\ i_{ec} \end{bmatrix} + \frac{c_1}{L_l} \begin{bmatrix} i_{ea} \\ i_{eb} \\ i_{ec} \end{bmatrix} + \frac{d_1}{L_l} \begin{bmatrix} e_a \\ e_b \\ e_c \end{bmatrix} \quad (5)$$

$$\begin{bmatrix} e_a \\ e_b \\ e_c \end{bmatrix} = \frac{a_2}{L_l} \begin{bmatrix} i_{sa} \\ i_{sb} \\ i_{sc} \end{bmatrix} + \frac{b_2}{L_l} \frac{d}{dt} \begin{bmatrix} i_{sa} \\ i_{sb} \\ i_{sc} \end{bmatrix} + \frac{c_2}{L_l} \begin{bmatrix} i_{ea} \\ i_{eb} \\ i_{ec} \end{bmatrix} + \frac{d_2}{L_l} \begin{bmatrix} V_{sa} \\ V_{sb} \\ V_{sc} \end{bmatrix} \quad (6)$$

where

$$\begin{aligned} a_1 &= (R_s L_l - R_l L_s) \\ b_1 &= -(L_s L_f + L_s L_l + L_l L_f) \\ c_1 &= -(R_f L_s + R_l L_s + R_f L_l) \\ d_1 &= (L_s + L_l) \\ a_2 &= -(R_s L_f + R_l L_f + R_s L_l) \\ b_2 &= -(L_s L_f + L_f L_l + L_l L_s) \\ c_2 &= (R_f L_l - R_l L_f) \\ d_2 &= (L_f + L_l). \end{aligned}$$

Transforming (5) and (6) to the synchronous reference frame and rearranging, we have

$$\frac{d}{dt} \begin{bmatrix} i_{sd} \\ i_{sq} \\ i_{ed} \\ i_{eq} \end{bmatrix} = \begin{bmatrix} -\frac{a_2}{b_2} & \omega & -\frac{c_2}{b_2} & 0 \\ -\omega & -\frac{a_2}{b_2} & 0 & -\frac{c_2}{b_2} \\ -\frac{a_1}{b_1} & 0 & -\frac{c_1}{b_1} & \omega \\ 0 & -\frac{a_1}{b_1} & -\omega & -\frac{c_1}{b_1} \end{bmatrix} \begin{bmatrix} i_{sd} \\ i_{sq} \\ i_{ed} \\ i_{eq} \end{bmatrix} + \begin{bmatrix} -\frac{d_2}{b_2} & 0 & \frac{L_l}{b_2} & 0 \\ 0 & -\frac{d_2}{b_2} & 0 & \frac{L_l}{b_2} \\ \frac{L_l}{b_1} & 0 & -\frac{d_1}{b_1} & 0 \\ 0 & \frac{L_l}{b_1} & 0 & -\frac{d_1}{b_1} \end{bmatrix} \begin{bmatrix} \sqrt{2}\,|v_s| \\ 0 \\ e_d \\ e_q \end{bmatrix} \quad (7)$$

where $|v_s|$ is the rms value of v_{sa}.

C. VSI DC-Side Model

The power balance equation of the VSI dc side and ac side is expressed as [5]

$$v_{\rm dc} i_{\rm dc} = \frac{3}{2}(e_d i_{ed} + e_q i_{eq}). \quad (8)$$

In addition, the dynamic equation for $v_{\rm dc}$ can be derived from a current balancing formula as follows:

$$\frac{d}{dt} v_{\rm dc} = -\left(\frac{v_{\rm dc}}{R_{\rm dc} C_{\rm dc}} + \frac{i_{\rm dc}}{C_{\rm dc}} \right). \quad (9)$$

From (8), the current $i_{\rm dc}$ in (9) can be expressed in terms of the state variables $v_{\rm dc}$, i_{ed}, and i_{eq} as follows:

$$i_{\rm dc} = \frac{3}{2 v_{\rm dc}}(e_d i_{ed} + e_q i_{eq}). \quad (10)$$

III. Design of Fixed-Gain PI Controller for STATCOM

With the dynamic model for the system at hand, we can proceed to design a fixed-gain PI controller for the STATCOM in order to regulate a load bus voltage under disturbance conditions. Fig. 2 shows the block diagram for the fixed-gain PI controller for the STATCOM [5], [7]–[9].

It is observed from Fig. 2 that the STATCOM controller is composed of four fixed-gain PI controllers: the d-axis current regulator, the q-axis current regulator, the dc voltage regulator, and the ac voltage regulator.

The primary function of the d- and q-axis current regulators is to regulate the d- and q-axis inverter currents i_{ed} and i_{eq} to the desired values i_{ed}^* and i_{eq}^* by adjusting the inverter output voltages e_d and e_q. The desired MI and angle α can be computed from these inverter output voltages e_d and e_q, as shown in the figure. Note that the d-axis is aligned to the load voltage v_l in the PI controller design process, while the d-axis for solving the VSI ac-side equations in (7) is aligned to the source voltage v_s. As a result, the computed phase angle α must be augmented by the phase angle difference between v_s and v_l, i.e., θ, before it is sent to the PWM generator to generate the switching pulses for the inverter switches in order to have correct phases for the inverter output ac voltages e_a, e_b, and e_c.

The dc voltage $v_{\rm dc}$ for the dc capacitor is regulated to the desired value $v_{\rm dc}^*$ by the dc voltage regulator. On the other hand, the load voltage $|v_l|$ is kept at the desired value $|v_l|^*$ by the ac voltage regulator.

Details on the design of the four regulators have been described in [7]–[9]. It has been found in [7]–[9] that, as far as the dynamic performance for load bus voltage regulation under disturbance conditions is concerned, the controller gains for the ac voltage regulator, i.e., K_P and K_I, play a more important role than those for the other three regulators. As a result, only the design of the controller gains for the ac voltage regulator is discussed in this paper.

To determine proper gains for the PI controllers, the nonlinear dynamic equations (7) and (9) for the system are linearized

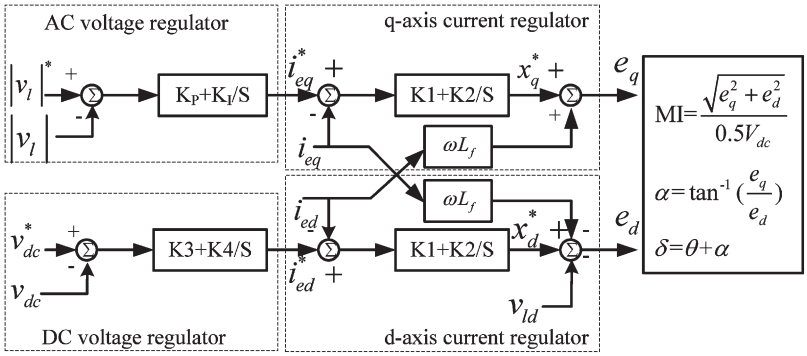

Fig. 2. Fixed-gain PI controller for the STATCOM.

TABLE II
SYSTEM PARAMETERS USED IN EXPERIMENT

Parameters	Values
Fundamental frequency	f=60Hz
Source voltage	v_s=78V_{peak}(55$V_{(rms)}$)
Source resistance	R_s=0.7Ω
Source inductance	L_s=1.6mH
Filter resistance	R_f=0.4Ω
Filter inductance	L_f=12mH
Switching frequency	f_c=1260Hz
DC capacitor	C_{dc}=2700μF
Estimated inverter loss resistance	R_{dc}=5000Ω
Sampling frequency	f_s=15360Hz

TABLE III
SYSTEM EIGENVALUES UNDER HEAVY LOAD CONDITION

System with STATCOM but without PI controller	System with STATCOM and with PI controller (K1=15, K2=15, K3=-1, K4=-5, K_P=-0.1, K_I=-17)
-264.21±j349	-748.92±j175
-5.05±j387	-170.42±j387
-0.15	-217.53
	-8.28
	-5.34
	-1.02
	-0.99

around a nominal loading condition, and the resulting linearized state equation is given by

$$\dot{X}(t) = AX(t) + BU(t) \tag{11}$$

where $X(t) = [i_{sd} \quad i_{sq} \quad i_{ed} \quad i_{eq} \quad v_{\rm dc}]^{\rm T}$ is the state vector and $U(t) = [e_d \quad e_q]^{\rm T}$ is the control vector. In this paper, heavy load condition is chosen as the nominal operating condition. The parameters for the system under study are listed in Table II, and eigenvalues for the system with STATCOM but without STATCOM controller are listed in column 1 of Table III.

It is observed from Table III that the STATCOM mode characterized by the pair of eigenvalues $-5.05 \pm j387$ has less damping than the others and that the eigenvalues for this mode should be shifted leftward to better locations by a STATCOM controller.

By using the method described in [7]–[9], the following controller gains for the PI controllers are obtained: $K1 = 15$, $K2 = 15$, $K3 = -1$, $K4 = -5$, $K_P = -0.1$, and $K_I = -17$.

The eigenvalues for the system with PI controllers are listed in column 2 of Table III. It is observed that the eigenvalues for the STATCOM mode have been shifted leftward from $-5.05 \pm j387$ to $-170.42 \pm j387$. Significant improvement in the damping for this mode has been achieved.

IV. DESIGN OF SELF-TUNING STATCOM CONTROLLER USING PSO

In the design of the fixed-gain STATCOM controller in the previous section, the PI controller gains K_P and K_I have been determined based on a particular loading condition (heavy load condition in this paper), and these gains are fixed in daily operation of the STATCOM.

Since these controller gains have been designed to give good dynamic responses for that particular loading condition, it may happen that unsatisfactory responses are observed as load changes with time. Thus, it is desirable to adjust the PI controller gains when there is a significant change in system load. In this paper, the PI controller gains K_P and K_I are adjusted by the PSO self-tuning controller as shown in Fig. 3.

The procedures followed by the proposed PSO self-tuning STATCOM controller to adjust the PI controller gains are summarized in Fig. 4 [26]–[28]. Details for these procedures are described as follows.

1) Determine Stable Regions for PI Controller Gains K_P and K_I: In the design of the self-tuning PI controller for the STATCOM, it is essential for the system to remain stable when the PI controller gains are adapted by the PSO algorithm. Therefore, the stable regions for the PI controller gains K_P and K_I must be first determined. This is done by computing the eigenvalues of the linearized state equation (11) for all possible combinations of K_P and K_I. The results are shown in Fig. 5 where the stable regions are depicted for the system with heavy load, medium load, and light load, respectively.

It is observed that the stable region expands as load is decreased. To ensure system stability under all possible loading conditions, the stable regions for the system with heavy load are adopted.

2) Measure Load Voltage v_l and Current i_l: The three phase load voltages $v_{la}(t)$, $v_{lb}(t)$, and $v_{lc}(t)$ and currents $i_{la}(t)$, $i_{lb}(t)$, and $i_{lc}(t)$ are measured with a sampling period of 1/15360 s, which is equivalent to 256 samples per cycle for a 60-Hz system. The analog signals fetched by the Hall sensors are first converted to digital signals through a multichannel data

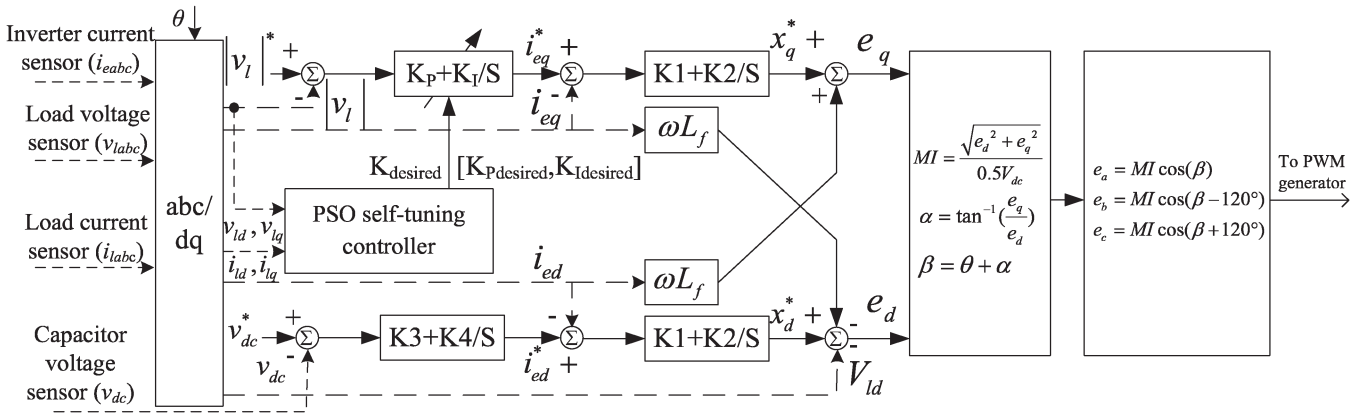

Fig. 3. Block diagram of the proposed PSO self-tuning STATCOM controller.

acquisition card, as shown in Fig. 1, before they are sent to the digital computer.

3) Estimate Load Impedance: To estimate the equivalent load resistance R_l and inductance L_l, the measured three phase load voltages $v_{la}(t)$, $v_{lb}(t)$, and $v_{lc}(t)$ and currents $i_{la}(t)$, $i_{lb}(t)$, and $i_{lc}(t)$ are first transformed to d- and q-axis components v_{ld}, v_{lq}, i_{ld}, and i_{lq} using the transformation matrix T in (2). Then, the desired values for R_l and L_l can be derived from (3), and the results are given as follows:

$$R_l = \frac{v_{ld}(\dot{i}_{lq}+\omega i_{ld}) - v_{lq}(\dot{i}_{ld}-\omega i_{lq})}{i_{ld}(\dot{i}_{lq}+\omega i_{ld}) - i_{lq}(\dot{i}_{ld}-\omega i_{lq})} \tag{12}$$

$$L_l = \frac{i_{ld}v_{ld} - i_{lq}v_{lq}}{i_{ld}(\dot{i}_{lq}+\omega i_{ld}) - i_{lq}(\dot{i}_{ld}-\omega i_{lq})} \tag{13}$$

where $\omega = 377$ rad/s for a 60-Hz system. Note that (14) and (15) can be used to estimate the impedance for an $R-C$ load

$$R_l = \frac{v_{ld}(\dot{v}_{lq}+\omega v_{ld}) - v_{lq}(\dot{v}_{ld}-\omega v_{lq})}{i_{ld}(\dot{v}_{lq}+\omega i_{ld}) - i_{lq}(\dot{v}_{ld}-\omega v_{lq})} \tag{14}$$

$$C_l = \frac{i_{lq}v_{ld} - i_{ld}v_{lq}}{v_{ld}(\dot{v}_{lq}+\omega i_{ld}) - v_{lq}(\dot{v}_{ld}-\omega v_{lq})}. \tag{15}$$

In this case, the dynamic equation (7) for an $R-L$ load must be replaced by (A.1) in Appendix A.

The voltage and current harmonics have only a minor effect on the estimated impedance and the resultant controller gains since they are filtered out by a low-pass filter.

4) Check if There Is a Significant Change in R_l and L_l: When there is no significant change in system load, it is not necessary to update the PI controller gains $K_{P\text{desired}}$ and $K_{I\text{desired}}$. These controller gains are updated when there is a change of more than 1% in system load impedance $|Z_l| = |R_l + j\omega L_l|$.

5) Update $K_{\text{desired}} = [K_{P\text{desired}} \quad K_{I\text{desired}}]^{\text{T}}$ using the PSO Algorithm: When there is a significant change in the system load, the following steps are followed to update the PI controller gains $K_{P\text{desired}}$ and $K_{I\text{desired}}$.

Step 1) Determine initial particle positions $K_P^{(0)}$, velocities $V_P^{(0)}$, and weight $w^{(0)}$. As shown in Fig. 6, the PSO algorithm begins with the selection of initial positions $K_P^{(0)}$, initial velocities $V_P^{(0)}(P = 1,\ldots,10)$ for the ten particles, and weight $w^{(0)} = 1.5$ at iteration 0. In this paper, ten particles were used for each iteration, and a total of 21 iterations were executed by the PSO algorithm. Note that the number of particles and number of iterations were selected such that satisfactory gains could be achieved in a short period. The initial positions (controller gains) $K_P^{(0)} = [K_{P_P}^{(0)} \quad K_{I_P}^{(0)}]^{\text{T}}$ were selected randomly within the stable regions for PI controller gains. On the other hand, the initial velocities (controller gain increments) $V_P^{(0)} = [\Delta K_{P_P}^{(0)} \quad \Delta K_{I_P}^{(0)}]^{\text{T}}$ were selected randomly between -1 and 1.

Step 2) Determine the best particle positions $Pbest = K_{P(pbest)}$ and the best global position $gbest = K_{(gbest)}$ for initial particle positions $K_P^{(0)}$. The performance of the system with the PI controller gains K_P and K_I can be described by the evaluation function E defined as

$$\begin{aligned} E &= \int ||v_l|^* - |v_l(t)||\, dt \\ &= \int \left||v_l|^* - \sqrt{v_{ld}(t)^2 + v_{lq}(t)^2}\right| dt \\ &\approx \sum_{j=1}^{2561} \left||v_l|^* - \sqrt{v_{ld}(j)^2 + v_{lq}(j)^2}\right| \Delta t \end{aligned} \tag{16}$$

where Δt is the sampling period (1/15360 s).

Note that the integral of absolute error (IAE) in load bus voltage $|v_l|$ has been employed as the evaluation function. It has been mentioned that a controller with minimum IAE will result in a response with relatively small overshoot and short rising time [35]. Thus, satisfactory stability, as well as fast response, can be achieved by the proposed controller designed using IAE criterion.

In this paper, the IAE is approximated by the sum of the error of v_l in the first 2560 samples (10 cycles or 167 ms) following the load change since it has been observed in our previous experiments that the load bus voltage $|v_l|$ returns to its desired value $|v_l|^*$ in less than ten cycles in most cases by using the proposed STATCOM. The samples $v_{ld}(j)$ and $v_{lq}(j)$

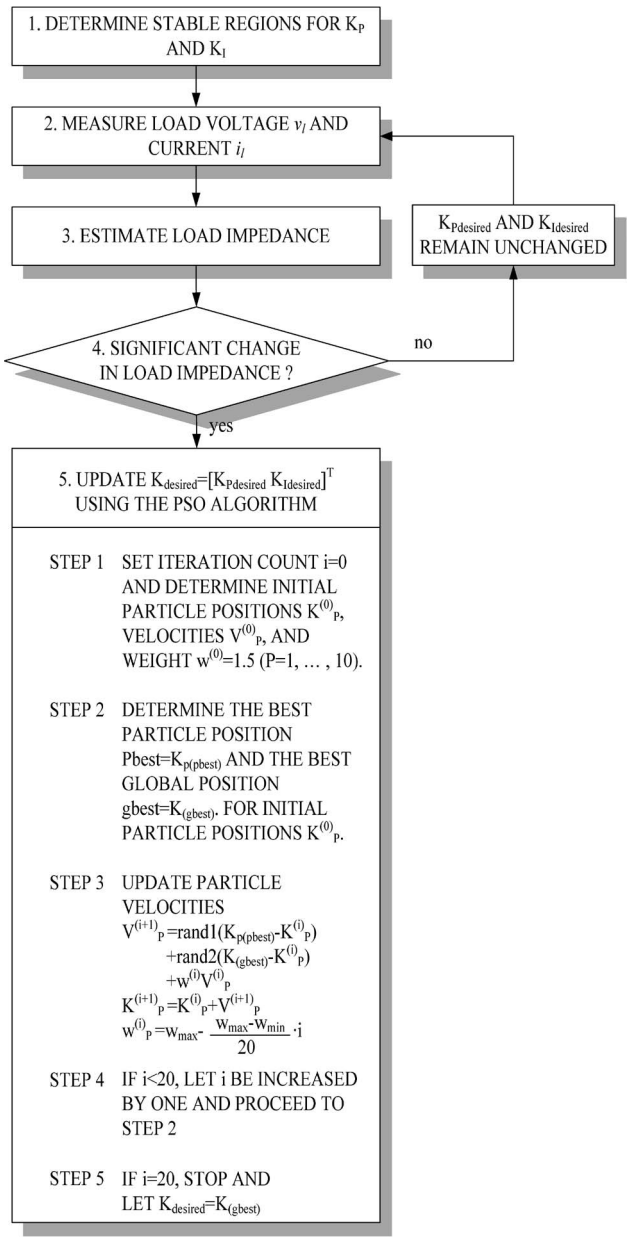

Fig. 4. Flowchart for the procedures of adjusting PI controller gains by the PSO self-tuning STATCOM controller.

used in the evaluation function are obtained by using the Runge–Kutta method [37] as soon as a change in system load is identified.

In the iteration process of the PSO algorithm, the best solution with the smallest evaluation function achieved so far by particle P is defined as the best particle position $Pbest = K_{P(pbest)} = [K_{P_{P(pbest)}} \quad K_{I_{P(pbest)}}]^{\mathrm{T}}$ for particle P. The best global position $gbest = K_{(gbest)} = [K_{P_{(gbest)}} \quad K_{I_{(gbest)}}]^{\mathrm{T}}$ is defined as the best solution with the smallest evaluation function achieved so far by all particles.

In the beginning of the iteration process, let us define $Pbest = K_{P(pbest)} = [K_{P_{P(pbest)}} \quad K_{I_{P(pbest)}}]^{\mathrm{T}} = [K^{(0)}_{P_P} \quad K^{(0)}_{I_P}]^{\mathrm{T}}$ and

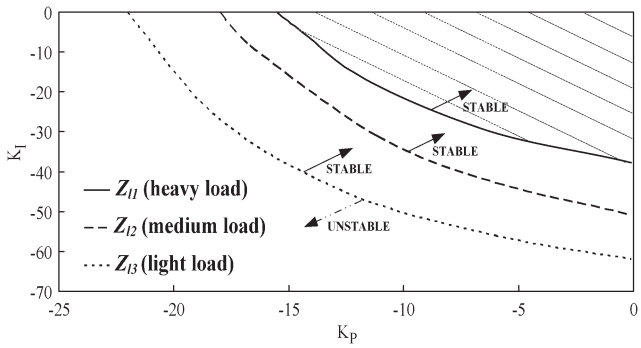

Fig. 5. Stable regions for K_P and K_I under different loading conditions.

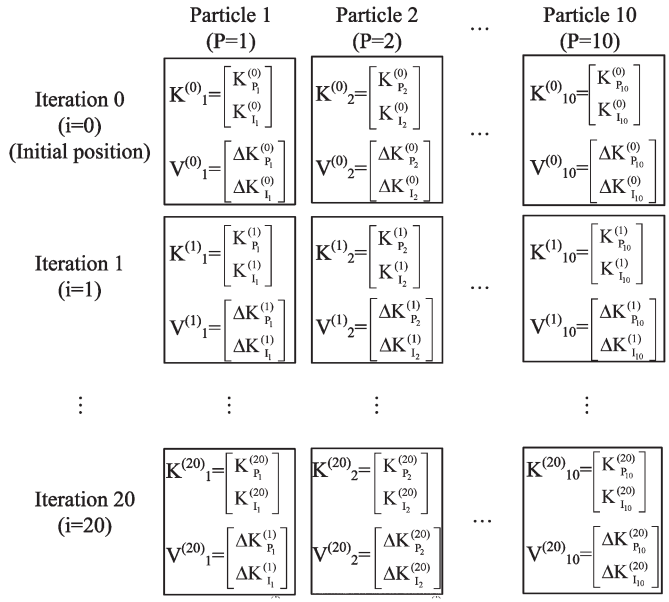

Fig. 6. Particle positions $K^{(i)}_P$ and velocities $V^{(i)}_P$ in the iteration process of PSO algorithm.

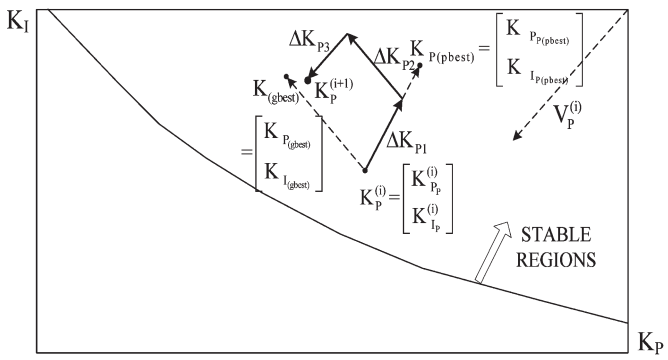

Fig. 7. Vector diagram showing how the position $K^{(i)}_P$ for particle P is updated in the PSO.

$gbest = K_{(gbest)} =$ the initial particle position $K^{(0)}_P (P = 1, \ldots, 10)$ with the smallest evaluation function E.

Step 3) Update particle velocities $V^{(i+1)}_P$, positions $K^{(i+1)}_P$, and weight $w^{(i)}$. For a particle P at iteration $i+1$, its position $K^{(i+1)}_P = [K^{(i+1)}_{P_P} \quad K^{(i+1)}_{I_P}]^{\mathrm{T}}$ and velocity $V^{(i+1)}_P = [\Delta K^{(i+1)}_{P_P} \quad \Delta K^{(i+1)}_{I_P}]^{\mathrm{T}}$ can be

computed using the particle position $K_P^{(i)}$ and velocity $V_P^{(i)}$ in the previous iteration and the distance from $K_P^{(i+1)}$ to $Pbest = K_{P(pbest)}$ and $gbest = K_{(gbest)}$ as follows:

$$K_P^{(i+1)} = K_P^{(i)} + V_P^{(i+1)} \tag{17}$$

$$V_P^{(i+1)} = rand1\left(K_{P(pbest)} - K_P^{(i)}\right) + rand2\left(K_{(gbest)} - K_P^{(i)}\right) + w^{(i)}V_P^{(i)} \tag{18}$$

where $rand1$ and $rand2$ are random numbers between 0 and 1 and

$$w^{(i)} = w_{\max} - \frac{w_{\max} - w_{\min}}{20} \cdot i. \tag{19}$$

Note that the weight $w^{(i)}$ for velocity decreases from $w_{\max}$ (=1.5 in this paper) to $w_{\min}(= 0.5)$ in the PSO iteration process.

The physical meanings implied in the update formulas (17) and (18) can be explained by the vector diagram in the $K_P - K_I$ plane as shown in Fig. 7. As shown in the figure, the position for particle P, i.e., $K_P^{(i+1)}$, is modified as follows:

$$K_P^{(i+1)} = K_P^{(i)} + \Delta K_P^{(i+1)} = K_P^{(i)} + V_P^{(i+1)} \tag{20}$$

where

$$\Delta K_P^{(i+1)} = \Delta K_{P1} + \Delta K_{P2} + \Delta K_{P3}$$

$$\Delta K_{P1} = rand1\left(K_{P(pbest)} - K_P^{(i)}\right)$$

= a vector from previous position $K_P^{(i)}$ toward the best particle position $K_{P(pbest)}$.

$$\Delta K_{P2} = rand2\left(K_{(gbest)} - K_P^{(i)}\right)$$

= a vector from previous position $K_P^{(i)}$ toward the best global position $K_{(gbest)}$.

$$\Delta K_{P3} = w^{(i)}V_P^{(i)}$$

= a vector which is in the direction of the velocity (position increment) in the previous iteration $\left(V_P^{(i)}\right)$.

Thus, the particle position in the $K_P - K_I$ plane is moved toward the best particle position $K_{P(pbest)}$ as well as the best global position $K_{(gbest)}$ in the PSO iteration process. In addition, the position increment $V_P^{(i)} = \Delta K_P^{(i)}$ in the previous iteration is also taken into account.

If the evaluation function E for the updated position $K_P^{(i+1)}$, i.e., $E(K_P^{(i+1)})$, is smaller than $E(K_{P(pbest)})$, then $K_P^{(i+1)}$ is selected as the new best particle position $K_{P(pbest)}$. In the same way, the best global position $K_{(\text{gest})}$ must be redefined based on the evaluation functions for all particle positions in the present and all previous iterations.

Step 4) The procedures in step 3) are repeated for 21 iterations.

Step 5) The desired PI controller gains $K_{\text{desired}} = [K_{P\text{desired}} \quad K_{I\text{desired}}]^{\text{T}}$ are chosen as the best global position $K_{(\text{gbset})} = [K_{P(gbest)} \quad K_{\text{I}(gbest)}]^{\text{T}}$.

TABLE IV
SIMULATED RESULTS OF DC CAPACITOR VOLTAGE LEVELS AND STATCOM RATING FOR STATCOM AT DIFFERENT VOLTAGE LEVELS

Voltage Level		STATCOM VAR Output		DC Capacitor Voltage Level		STATCOM Rating	
22.8*	(KV)	+40	(MVAR)	58.3	(KV)	40.0	(MVA)
		+20	(MVAR)	51.1	(KV)	20.0	(MVA)
11.4*	(KV)	+20	(MVAR)	35.2	(KV)	20.0	(MVA)
		+10	(MVAR)	28.7	(KV)	10.0	(MVA)

* DISTRIBUTION VOLTAGE LEVEL

V. EXPERIMENTAL RESULTS

To demonstrate the effectiveness of the proposed PSO self-tuning STATCOM controller in regulating load bus voltage under different loading conditions, a prototype 1.5-kVA STATCOM for a scale-down distribution system has been implemented at the laboratory. Note that the voltage level has been reduced to 55 V (rms) at the laboratory. However, the control algorithm presented in this paper can be applied to STATCOMs in a real distribution system with a higher voltage. Simulated results of dc capacitor voltage levels and STATCOM ratings for STATCOM at different voltage levels are summarized in Table IV. These results can also be achieved using (B.5) and (B.6) in Appendix B. It is observed from Table IV that a higher dc capacitor voltage v_{dc} must be used when the STATCOM is applied to a real distribution system with a higher voltage since the inverter output voltage is proportional to the product of the MI and the dc capacitor voltage (v_{dc}) and MI is normally maintained at a value close to one [38]. In addition, power switches with higher voltage and current ratings must be adopted. However, the control algorithm remains the same.

The system configuration for the experimental setup has been shown in Fig. 1. The system parameters used in the experiments have been given in Table II. Three different loading conditions were examined in the experiments.

1) Heavy load: $Z_{l1} = 3.84 + j7.55\ \Omega$.
2) Medium load: $Z_{l2} = 8.4 + j15.08\ \Omega$.
3) Light load: $Z_{l3} = 15.4 + j30.16\ \Omega$.

A. Speed and Accuracy of Numerical Solutions of Evaluation Function

It was mentioned earlier that the evaluation function in (16) should be computed rapidly and accurately for each particle position in the PSO algorithm such that good solutions for the controller gains could be reached in a very short period following a load change. A numerical simulation program was written on a digital computer to simulate the dynamic voltage response under disturbance condition using the Runge–Kutta method [37]. It was found that the dynamic responses for all the

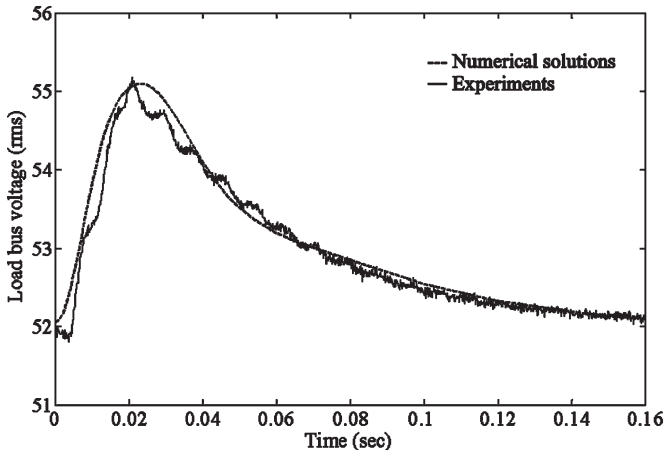

Fig. 8. Comparison of the dynamic responses from numerical simulations and experiments.

particle positions in the PSO algorithm can be reached within one sampling period (1/15360 s). Thus, the controller gains can be determined in a short period of 1/15360 s following the load change.

To demonstrate the accuracy of the numerical solutions for the dynamic responses, Fig. 8 shows the dynamic voltage responses for the load bus voltage when the load is changed from heavy load to light load. A comparison of the response curves from numerical simulations and experiments reveals that the response from numerical simulations matches closely to that from experiments. Thus, it is concluded that the evaluation function E required in the PSO algorithm can be reached by the numerical simulation program in an accurate and efficient manner.

B. Dynamic Response

To examine the dynamic response of the proposed self-tuning STATCOM controller with PSO adaptation scheme, three tests were conducted at the laboratory.

1) System load was decreased from heavy load to light load at $t = 1$ s.
2) System load was decreased from heavy load to medium load at $t = 1$ s.
3) System load was decreased from medium load to light load at $t = 1$ s.

The experimental results from the three tests are shown in Figs. 9–11, respectively. A comparison of the dynamic response curves of the load bus voltage in Fig. 9(a) for test 1 reveals that the load bus voltage returned to the preset values of 52 V(rms) in 0.1 s following the disturbance for the STATCOM with the self-tuning controller. On the other hand, it took about 0.16 s for the STATCOM with the fixed-gain PI controller to return to the preset voltage. The maximum voltage was also reduced from 55.3 to 54.6 V when the PSO self-tuning controller was employed to replace the fixed-gain PI controller which was designed using pole-assignment method. Note that accurate voltage and current response are fetched by the Hall sensors and transmitted to the digital computer through A/D converters. The sensor includes a Hall element, an OP amplifier circuit, an offset circuit, and a low-pass filter. It is

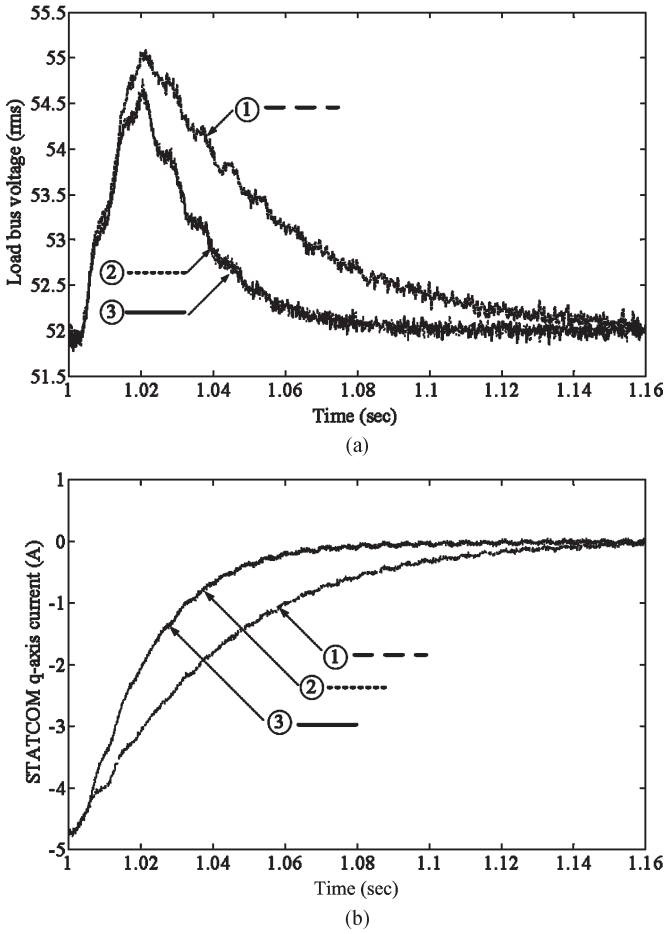

①--- Fixed-gain PI controller (pole assignment in Table III).
②… Fixed-gain PI controller (K_P and K_I are the same as those for the PSO at heavy load).
③— PSO self-tuning PI controller.

Fig. 9. Dynamic responses for test 1.

observed from the waveforms in Fig. 9 that the noise levels are less than 50 mV and the difference between the maximum signal voltage levels of 55.3 and 54.6 V can be identified. If the PI controller gains were fixed at the values reached by the PSO under heavy load, the fixed-gain PI controller gave similar response curves with the PSO self-tuning PI controller. However, better dynamic responses were achieved by the PSO self-tuning controller than the two fixed-gain PI controllers as the load was changed from heavy load to medium load or light load, as shown in Figs. 10 and 11.

An observation of the response curves in Fig. 9(b) indicates that the STATCOM q-axis current i_{eq} returned from 4.7 to 0 A in about 0.1 s for the self-tuning controller, and it took about 0.16 s for i_{eq} to return to 0 A for the fixed-gain PI controller.

It is thus concluded from the experimental results in Figs. 9–11 that faster response with less overshoot can be achieved by the proposed PSO self-tuning PI controller than by the fixed-gain PI controller under changing loading conditions.

C. Steady-State Performance

The steady-state responses of the PSO self-tuning STATCOM controller for the system under light load, medium

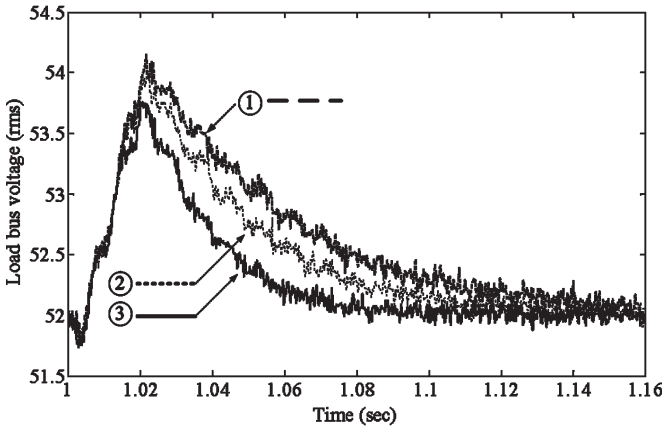

①--- Fixed-gain PI controller (pole assignment in Table III).
②… Fixed-gain PI controller (K_P and K_I are the same as those for the PSO at heavy load).
③— PSO self-tuning PI controller.

Fig. 10. Dynamic responses for test 2.

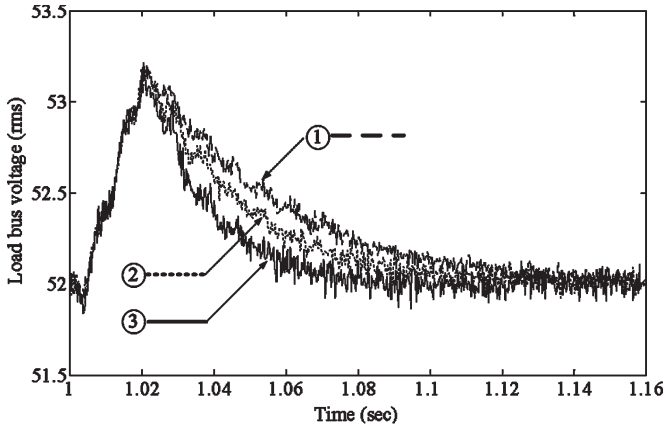

①--- Fixed-gain PI controller (pole assignment in Table III).
②… Fixed-gain PI controller (K_P and K_I are the same as those for the PSO at heavy load).
③— PSO self-tuning PI controller.

Fig. 11. Dynamic responses for test 3.

load, and heavy load conditions are shown in Figs. 12–14, respectively. An observation of the load bus voltages in the three figures indicates that the load bus voltage remained constant at the preset value of 52 V(rms). It is also observed that the voltage for the dc capacitor $v_{\rm dc}$ remained constant at the specified value of 220 V.

When the load is increased from light load to medium load and to heavy load, it is necessary for the STATCOM to deliver more reactive power to the system in order to maintain constant voltage at the load bus. This can be achieved by increasing the inverter output voltage e_a and reactive output current i_{ea}. Since e_a is proportional to $v_{\rm dc}$ and the MI [5], [7], it is observed from Figs. 12–14 that MI was increased from 0.65 at light load to 0.8 at medium load and to 0.89 at heavy load.

The inverter output voltage e_a was increased from 71.5 V at light load to 88 V at medium load and to 97.9 V at heavy load. The inverter output current i_{ea} was increased from 0.1 A at light load to 2.4 A at medium load and to 4.8 A at heavy load. In addition, it is observed from these figures that i_{ea} lagged v_{la} by an angle of $\phi \approx 90^\circ$ since the STACOM real power loss was relatively small compared with its output reactive power.

D. System With Nonlinear Load

Experiments were also conducted for the system in Fig. 15 to examine the effectiveness of the proposed PSO self-tuning STATCOM controller in a system with a nonlinear load, which comprises a three-phase bridge rectifier and a resistive load. The dynamic responses of the PSO self-tuning STATCOM controller for test 1 with nonlinear load included, test 2 with nonlinear load included, and test 3 with nonlinear load included are shown in Figs. 16–18, respectively. Table V summarizes the percentage apparent power of the linear and nonlinear loads under these different conditions. The steady-state responses of the PSO self-tuning STATCOM controller for the system under linear light load and nonlinear load condition, linear medium load and nonlinear load condition, and linear heavy load and nonlinear condition are shown in Figs. 19–21, respectively. Note that the equivalent resistance and inductance (or capacitance) of the system with a nonlinear load are estimated using the same formulas (12)–(15) for the system with nonlinear load. The only difference is that a low-pass filter must be designed such that the harmonics in the measured ac voltages and currents are filtered out before the voltage and current signals are transformed to the d–q frame to obtain the variables

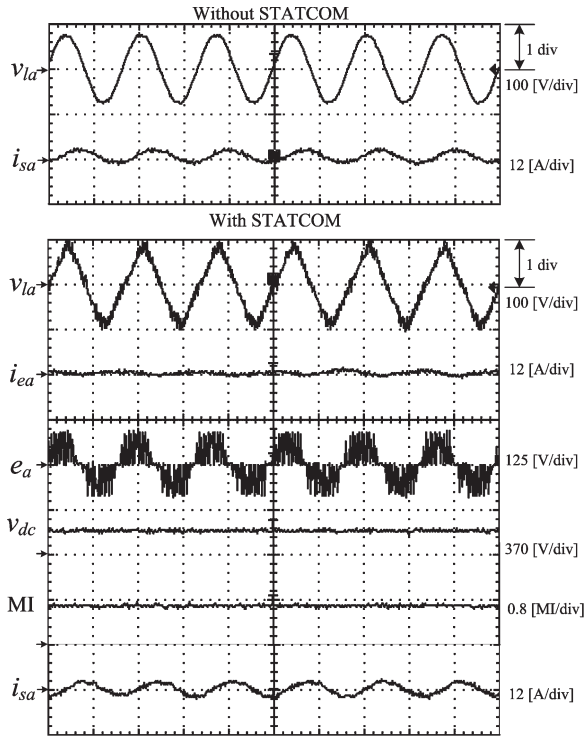

Fig. 12. Steady-state performance at light load.

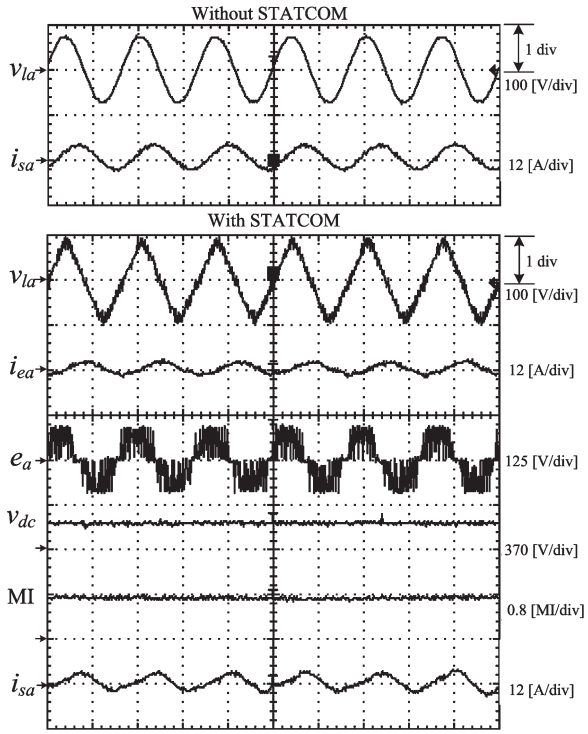

Fig. 13. Steady-state performance at medium load.

v_{ld}, v_{lq}, i_{ld}, and i_{lq} which are required in (12)–(15). When the equivalent reactive power is positive, (12) and (13) are used to estimate the equivalent resistance R_l and inductance L_l. On the other hand, (14) and (15) are used to estimate the equivalent resistance R_l and capacitance C_l when the equivalent reactive power is negative. It is observed from Figs. 16–21 that satisfac-

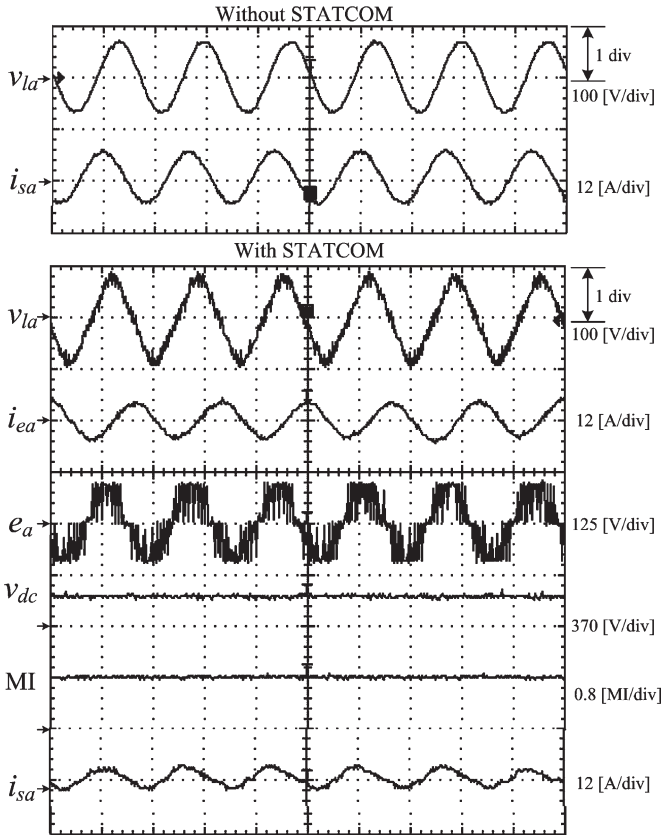

Fig. 14. Steady-state performance at heavy load.

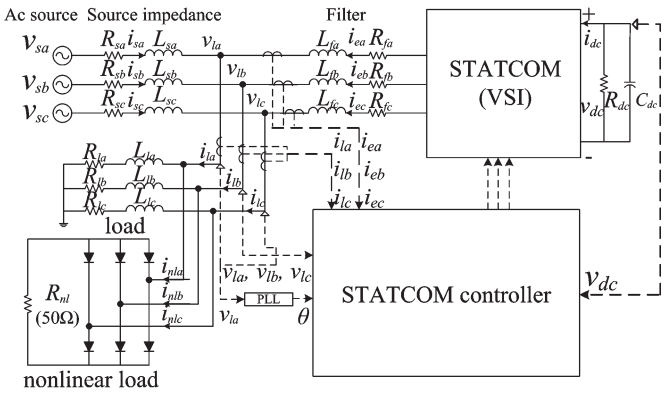

Fig. 15. System with nonlinear load.

tory responses are achieved by the PSO self-tuning STATCOM controller in a system with a nonlinear load.

VI. Conclusion

A self-tuning PI controller has been designed for a STATCOM using the PSO technique. When system load changes with time in daily operation of the STATCOM, the load impedance is first estimated from real-time measurements. Based on the estimated load impedance, the PSO technique is employed to adapt the PI controller gains. To speed up the gain adaptation procedure, an accurate and efficient digital simulation program using the Runge–Kutta method has been developed. In addition, the best particle gains, the best

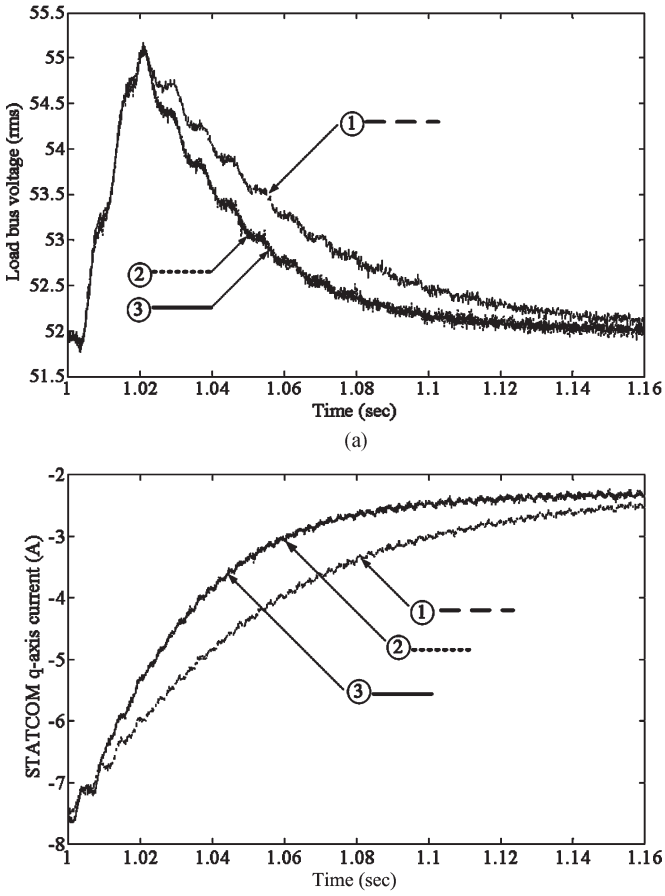

①--- Fixed-gain PI controller (Table III).
②… Fixed-gain PI controller (K_P and K_I are the same as those for the PSO at heavy load and nonlinear load).
③— PSO self-tuning PI controller.

Fig. 16. Dynamic responses for test 1 with nonlinear load included.

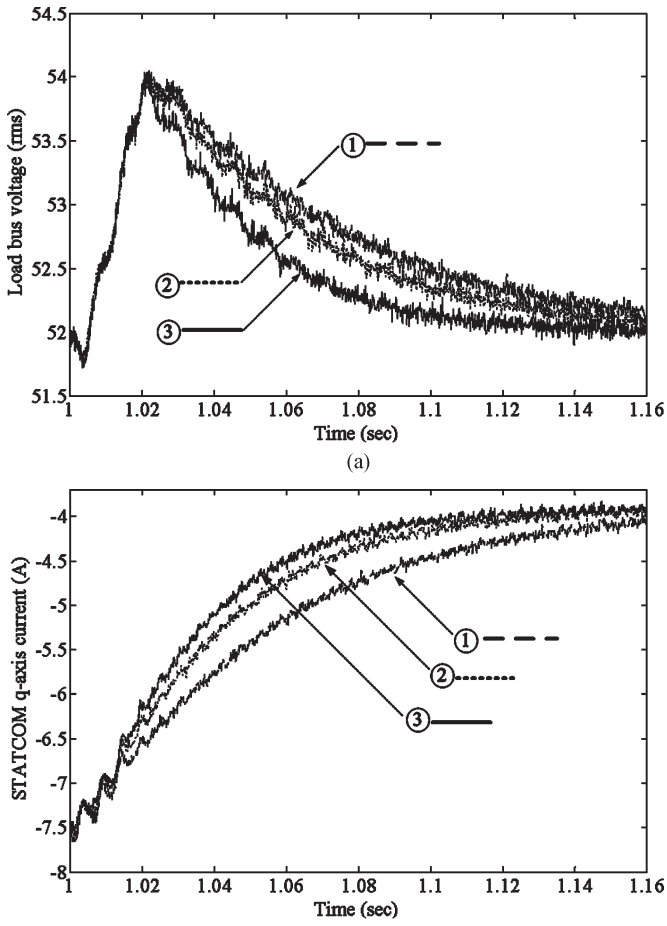

①--- Fixed-gain PI controller (Table III).
②… Fixed-gain PI controller (K_P and K_I are the same as those for the PSO at medium load and nonlinear load).
③— PSO self-tuning PI controller.

Fig. 17. Dynamic responses for test 2 with nonlinear load included.

global gains, and previous gain adjustments are all taken into account in the PSO algorithm. As a result, the desired gains can be achieved by the PSO in a very efficient manner, and the PI controller gains can be adjusted within a very short period following a change in system load. Experimental results for the system under different loading conditions have been presented to demonstrate the effectiveness of the proposed PSO self-tuning controller for the STATCOM. It is found that satisfactory dynamic responses can be reached by the proposed self-tuning controller under various loading conditions. It is also found that, with the controller gains adapted by the proposed PSO technique, better dynamic responses can be achieved by the self-tuning controller than the fixed-gain controller.

In this paper, the load impedance is computed directly from the measured voltages and currents. There is no need to estimate system dynamic equations using the method of recursive least squares [39], [40]. The controller gains are determined using the PSO algorithm based on dynamic responses of system voltage.

Only balanced loads have been considered in this paper. Future works will be devoted to the applications of the self-tuning controller to unbalanced loads.

APPENDIX

A. VSI AC-Side Model for $R-C$ Load

$$\frac{d}{dt}\begin{bmatrix} i_{sd} \\ i_{sq} \\ i_{ed} \\ i_{eq} \\ v_{ld} \\ v_{lq} \end{bmatrix} = \begin{bmatrix} -\frac{R_s}{L_s} & \omega & 0 & 0 & -\frac{1}{L_s} & 0 \\ -\omega & -\frac{R_s}{L_s} & 0 & 0 & 0 & -\frac{1}{L_s} \\ 0 & 0 & -\frac{R_f}{L_f} & \omega & -\frac{1}{L_f} & 0 \\ 0 & 0 & -\omega & -\frac{R_f}{L_f} & 0 & -\frac{1}{L_f} \\ \frac{1}{C_l} & 0 & \frac{1}{C_l} & 0 & -\frac{1}{C_l R_l} & \omega \\ 0 & \frac{1}{C_l} & 0 & \frac{1}{C_l} & -\omega & -\frac{1}{C_l R_l} \end{bmatrix} \begin{bmatrix} i_{sd} \\ i_{sq} \\ i_{ed} \\ i_{eq} \\ v_{ld} \\ v_{lq} \end{bmatrix} + \begin{bmatrix} \frac{1}{L_s} & 0 & 0 & 0 \\ 0 & \frac{1}{L_s} & 0 & 0 \\ 0 & 0 & \frac{1}{L_f} & 0 \\ 0 & 0 & 0 & \frac{1}{L_f} \\ 0 & 0 & 0 & 0 \\ 0 & 0 & 0 & 0 \end{bmatrix} \begin{bmatrix} \sqrt{2}|v_s| \\ 0 \\ e_d \\ e_q \end{bmatrix}. \quad \text{(A.1)}$$

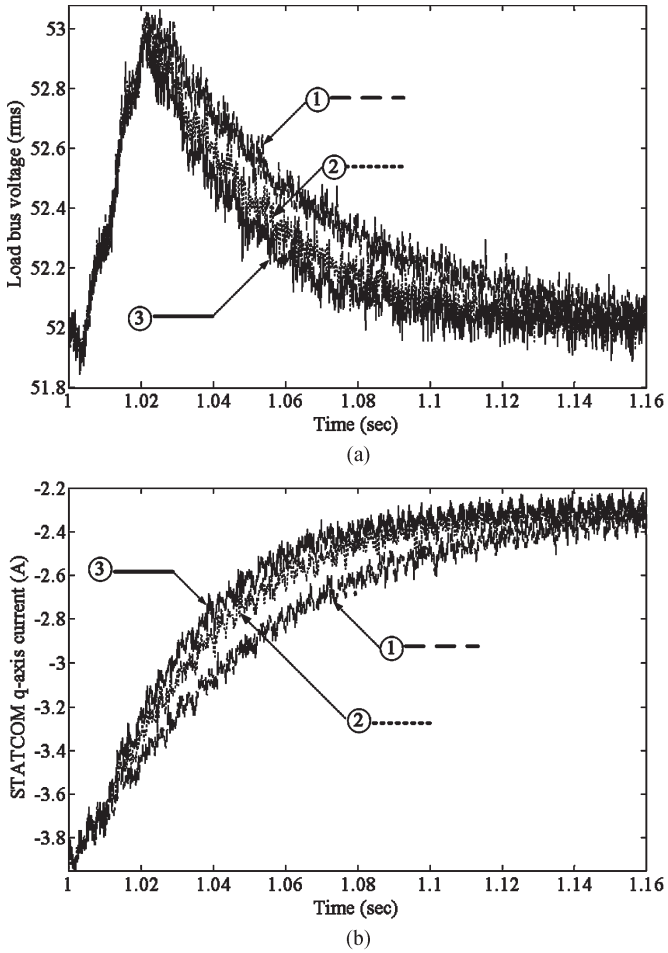

①--- Fixed-gain PI controller (Table III).
②… Fixed-gain PI controller (K_P and K_I are the same as those for the PSO at light load and nonlinear load).
③— PSO self-tuning PI controller.

Fig. 18. Dynamic responses for test 3 with nonlinear load included.

TABLE V
PERCENTAGE APPARENT POWERS OF LINEAR LOAD AND NONLINEAR LOAD

Load Condition	Linear Load	Nonlinear Load
Linear light load and Nonlinear load	22.4%	77.6%
Linear medium load and Nonlinear load	43.1%	56.9%
Linear heavy load and Nonlinear load	63.9%	36.1%

B. STATCOM Parameters at Different Voltage Levels

The dc capacitor voltage levels and STATCOM ratings for STATCOM at different voltage levels are derived as follows.

From Fig. 22, we have the voltage equations at the synchronous reference frame for the ac side

$$e_d = v_{ld} + R_f i_{ed} - \omega L_f i_{eq} \tag{B.1}$$

$$e_q = R_f i_{eq} + \omega L_f i_{ed}. \tag{B.2}$$

The inverter ac voltages e_d and e_q are related to the dc capacitor voltage $v_{\rm dc}$ from a power balancing formula as follows:

$$v_{\rm dc} i_{\rm dc} = \frac{3}{2}(e_d i_{ed} + e_q i_{eq}). \tag{B.3}$$

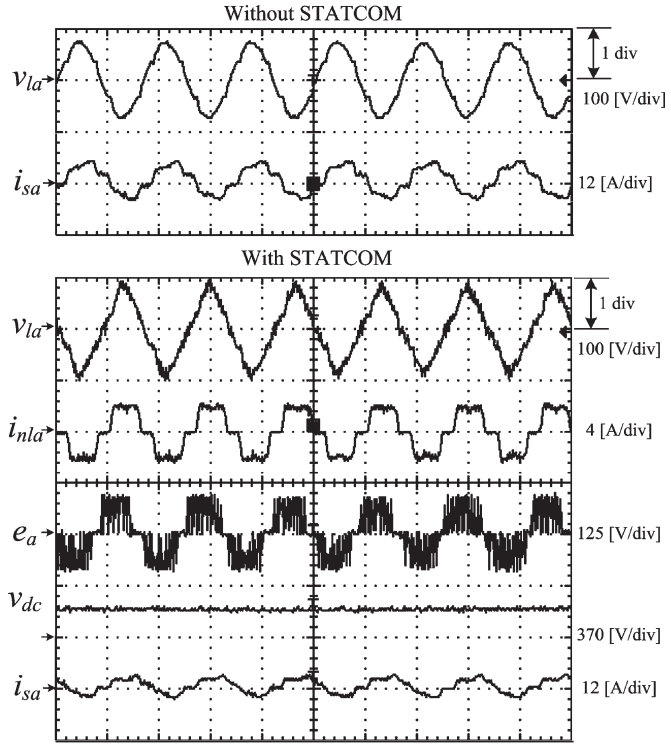

Fig. 19. Steady-state performance for the system with linear light load and nonlinear load.

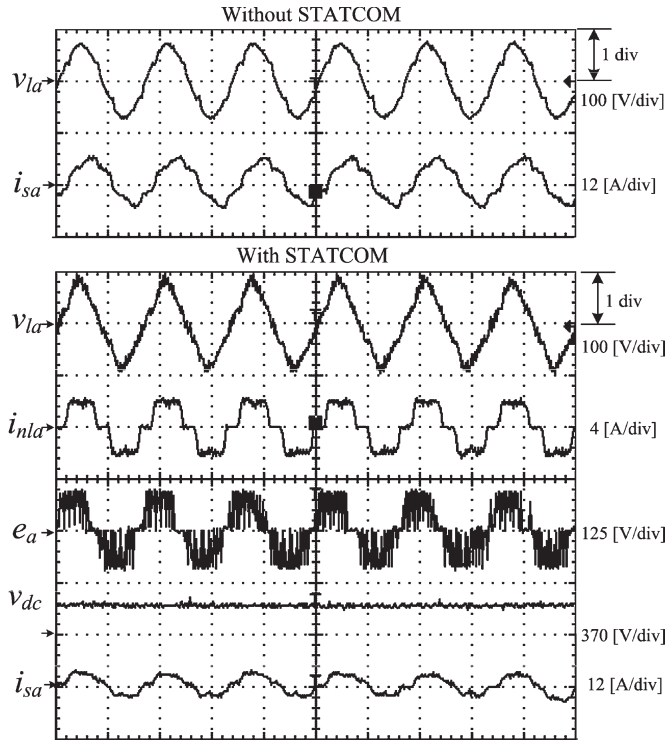

Fig. 20. Steady-state performance for the system with linear medium load and nonlinear load.

The reactive power delivered to the power system is given by

$$Q = -\frac{3}{2} v_{ld} i_{eq}. \tag{B.4}$$

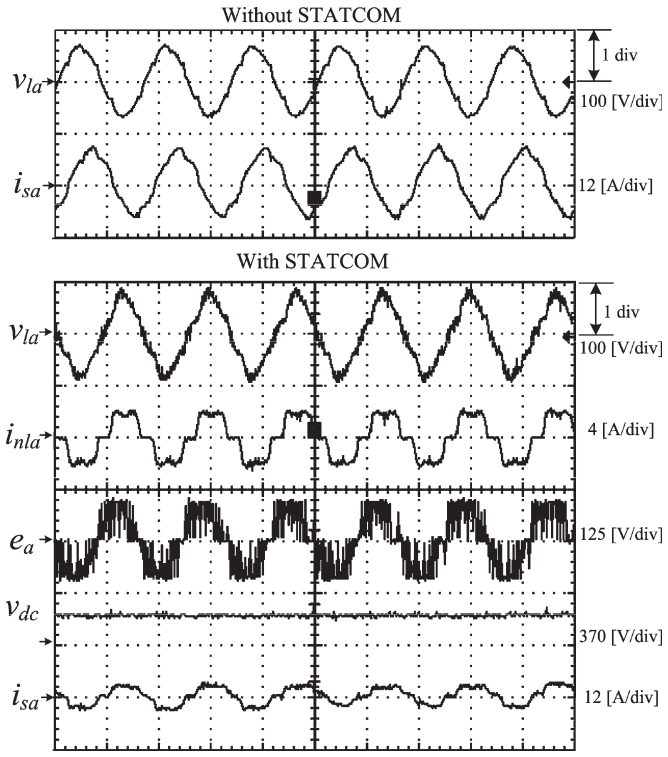

Fig. 21. Steady-state performance for the system with linear heavy load and nonlinear load.

Rearranging (B.1)–(B.4), we have

$$Q = X_1 + X_2 v_{\rm dc}^2 + \sqrt{X_3 v_{\rm dc}^2 + X_4 v_{\rm dc}^4} \tag{B.5}$$

$$v_{\rm dc} = \sqrt{Y_1 + Y_2 Q - \sqrt{Y_3 + Y_4 Q + Y_5 Q^2}} \tag{B.6}$$

where

$$X_1 = \frac{-\omega L_f v_{ld}^2}{Z_f^2} \quad \left(Z_f = \sqrt{R_f^2 + (\omega L_f)^2}\right)$$

$$X_2 = \frac{R_f \omega L_f \left(3R_{\rm dc} R_f + 8Z_f^2\right)}{6R_{\rm dc} Z_f^4}$$

$$X_3 = \frac{\left(R_f^2 - (\omega L_f)^2\right)^2 v_{ld}^2}{4Z_f^6}$$

$$X_4 = \frac{-\left(R_f^2 - (\omega L_f)^2\right)^2 \left(3R_{\rm dc} R_f + 8Z_f^2\right)^2}{144 R_{\rm dc}^2 Z_f^8}.$$

$$Y_1 = \frac{-2X_1 X_2 + X_3}{2\left(X_2^2 - X_4\right)}$$

$$Y_2 = \frac{2X_2}{2\left(X_2^2 - X_4\right)}$$

$$Y_3 = \frac{X_3^2 - 4X_1 X_2 X_3 + 4X_1^2 X_4}{4\left(X_2^2 - X_4\right)^2}$$

$$Y_4 = \frac{4X_2 X_3 - 8X_1 X_4}{4\left(X_2^2 - X_4\right)^2}$$

$$Y_5 = \frac{4X_4}{4\left(X_2^2 - X_4\right)^2}.$$

By using (B.5) and (B.6), the dc capacitor voltages for 11.4- and 22.8-kV systems were computed, and the results are shown as a dotted curve and solid curve, respectively, in Fig. 23. Note

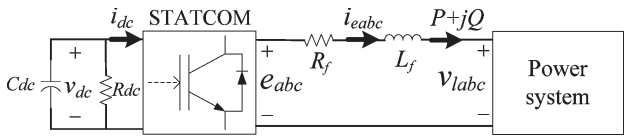

Fig. 22. One-line diagram of a STATCOM connected to a power system.

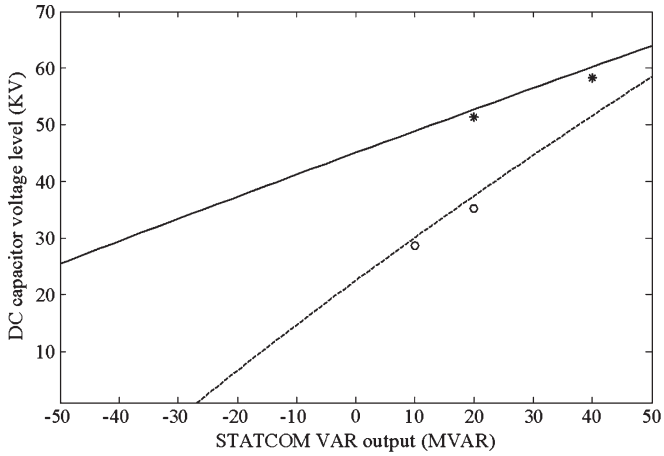

--- Computed DC capacitor voltage for 11.4 KV system.
— Computed DC capacitor voltage for 22.8 KV system.
○Simulated DC capacitor voltage for 11.4 KV system. (using MATLAB®/SIMULINK).
*Simulated DC capacitor voltage for 22.8 KV system. (using MATLAB®/SIMULINK).

Fig. 23. STATCOM VAR output versus dc capacitor voltage.

that (B.5) and (B.6) reduce to (B.7) and (B.8) when R_f and converter losses $(v_{\rm dc}^2/R_{\rm dc})$ are neglected

$$Q = \frac{3\left(v_{\rm dc} v_{ld} - 2v_{ld}^2\right)}{4\omega L_f} \tag{B.7}$$

$$v_{\rm dc} = \frac{4\omega L_f Q + 6v_{ld}^2}{3v_{ld}}. \tag{B.8}$$

MATLAB/SIMULINK was also employed to simulate the dc capacitor voltages for the 11.4- and 22.8-kV systems, and simulation results are also shown in Fig. 23. It is observed from Fig. 23 that the simulation results are close to the results from computations. The simulation results are also summarized in Table IV.

REFERENCES

[1] T. J. E. Miller, Ed., *Reactive Power Control in Electric Systems*. New York: Wiley, 1982.
[2] N. G. Hingorani and L. Gyugyi, *Understanding FACTS*. New York: IEEE Press, 2000.
[3] K. Acharya, S. K. Mazumder, and I. Basu, "Reaching criterion of a three-phase voltage-source inverter operating with passive and nonlinear loads and its impact on global stability," *IEEE Trans. Ind. Electron.*, vol. 55, no. 4, pp. 1795–1812, Apr. 2008.
[4] D. Dujic, G. Grandi, M. Jones, and E. Levi, "A space vector PWM scheme for multifrequency output voltage generation with multiphase voltage-source inverters," *IEEE Trans. Ind. Electron.*, vol. 55, no. 5, pp. 1943–1955, May 2008.
[5] C. Schauder and H. Mehta, "Vector analysis and control of advanced static VAR compensators," *Proc. Inst. Elect. Eng.—C*, vol. 140, no. 4, pp. 299–306, Jul. 1993.

[6] G. Joos, L. T. Moran, and P. D. Ziogas, "Performance analysis of a PWM inverter VAR compensator," *IEEE Trans. Power Electron.*, vol. 6, no. 3, pp. 380–391, Jul. 1991.
[7] B. S. Chen and Y. Y. Hsu, "A minimal harmonic controller for a STATCOM," *IEEE Trans. Ind. Electron.*, vol. 55, no. 2, pp. 655–664, Feb. 2008.
[8] B. S. Chen and Y. Y. Hsu, "An analytical approach to harmonic analysis and controller design of a STATCOM," *IEEE Trans. Power Del.*, vol. 22, no. 1, pp. 423–432, Jan. 2007.
[9] C. T. Chang and Y. Y. Hsu, "Design of an ANN tuned adaptive UPFC supplementary damping controller for power system dynamic performance enhancement," *Electr. Power Syst. Res.*, vol. 66, no. 3, pp. 259–265, Sep. 2003.
[10] B. Singh, S. S. Murthy, and S. Gupta, "STATCOM-based voltage regulator for self-excited induction generator feeding nonlinear loads," *IEEE Trans. Ind. Electron.*, vol. 53, no. 5, pp. 1437–1452, Oct. 2006.
[11] S. Mohagheghi, Y. del Valle, G. K. Venayagamoorthy, and R. G. Harley, "A proportional-integral type adaptive critic design-based neuro controller for a static compensator in a multimachine power system," *IEEE Trans. Ind. Electron.*, vol. 54, no. 1, pp. 86–96, Feb. 2007.
[12] S. Mohagheghi, R. G. Harley, and G. K. Venayagamoorthy, "An adaptive Mamdani fuzzy logic based controller for STATCOM in a multimachine power system," in *Proc. ISAP*, Nov. 2005, pp. 228–233.
[13] Y. Cheng, C. Qian, M. L. Crow, S. Pekarek, and S. Atcitty, "A comparison of diode-clamped and cascaded multilevel converters for a STATCOM with energy storage," *IEEE Trans. Ind. Electron.*, vol. 53, no. 5, pp. 1512–1521, Oct. 2006.
[14] D. Soto and T. C. Green, "A comparison of high-power converter topologies for the implementation of FACTS controllers," *IEEE Trans. Ind. Electron.*, vol. 49, no. 5, pp. 1072–1080, Oct. 2002.
[15] V. Dinavahi, R. Iravani, and R. Bonert, "Design of a real-time digital simulator for a D-STATCOM system," *IEEE Trans. Ind. Electron.*, vol. 51, no. 5, pp. 1001–1008, Oct. 2004.
[16] J. Dixon, Y. del Valle, M. Orchard, M. Ortuzar, L. Moran, and C. Maffrand, "A full compensating system for general loads, based on a combination of thyristor binary compensator, and a PWM-IGBT active power filter," *IEEE Trans. Ind. Electron.*, vol. 50, no. 5, pp. 982–989, Oct. 2003.
[17] B. K. Lee and M. Ehsani, "A simplified functional simulation model for three-phase voltage-source inverter using switching function concept," *IEEE Trans. Ind. Electron.*, vol. 48, no. 2, pp. 309–321, Apr. 2001.
[18] Y. W. Li, "Control and resonance damping of voltage-source and current-source converters with LC filters," *IEEE Trans. Ind. Electron.*, vol. 56, no. 5, pp. 1511–1521, May 2009.
[19] J. R. Espinoza, G. Joos, J. I. Guzman, L. A. Moran, and R. P. Burgos, "Selective harmonic elimination and current/voltage control in current/voltage-source topologies: A unified approach," *IEEE Trans. Ind. Electron.*, vol. 48, no. 1, pp. 71–81, Feb. 2001.
[20] B. M. Han and S. I. Moon, "Static reactive-power compensator using soft-switching current-source inverter," *IEEE Trans. Ind. Electron.*, vol. 48, no. 6, pp. 1158–1165, Dec. 2001.
[21] P. Flores, J. Dixon, M. Ortuzar, R. Carmi, P. Barriuso, and L. Moran, "Static VAR compensator and active power filter with power injection capability, using 27-level inverters and photovoltaic cells," *IEEE Trans. Ind. Electron.*, vol. 56, no. 1, pp. 130–138, Jan. 2009.
[22] V. F. Corasaniti, M. B. Barbieri, P. L. Arnera, and M. I. Valla, "Hybrid active filter for reactive and harmonics compensation in a distribution network," *IEEE Trans. Ind. Electron.*, vol. 56, no. 3, pp. 670–677, Mar. 2009.
[23] J. A. Barrena, L. Marroyo, M. A. R. Vidal, and J. R. T. Apraiz, "Individual voltage balancing strategy for PWM cascaded h-bridge converter-based STATCOM," *IEEE Trans. Ind. Electron.*, vol. 55, no. 1, pp. 21–29, Jan. 2008.
[24] Y. A.-R. I. Mohamed and E. F. El-Saadany, "A control scheme for PWM voltage-source distributed-generation inverters for fast load-voltage regulation and effective mitigation of unbalanced voltage disturbances," *IEEE Trans. Ind. Electron.*, vol. 55, no. 5, pp. 2072–2084, May 2008.
[25] S. Mohagheghi, G. K. Venayagamoorthy, and R. G. Harley, "Fully evolvable optimal neurofuzzy controller using adaptive critic designs," *IEEE Trans. Fuzzy Syst.*, vol. 16, no. 6, pp. 1450–1461, Dec. 2008.
[26] J. Kennedy and R. Eberhart, "Particle swarm optimization," in *Proc. IEEE Int. Conf. Neural Netw.*, Perth, Australia, Nov. 1995, vol. IV, pp. 1942–1948.
[27] J. Kennedy and R. Eberhart, "A new optimizer using particle swarm theory," in *Proc. 6th Int. Symp. Micromachine Human Sci.*, Nagoya, Japan, Oct. 1995, pp. 39–43.
[28] Y. Shi and R. Eberhart, "A modified particle swarm optimizer," in *Proc. IEEE Int. Conf. Evol. Comput.*, Anchorage, AK, May 1998, pp. 69–73.
[29] B. Biswal, P. K. Dash, and B. K. Panigrahi, "Power quality disturbance classification using fuzzy c-means algorithm and adaptive particle swarm optimization," *IEEE Trans. Ind. Electron.*, vol. 56, no. 1, pp. 212–220, Jan. 2009.
[30] F. J. Lin, L. T. Teng, J. W. Lin, and S. Y. Chen, "Recurrent functional-link-based-fuzzy-neural-network-controlled induction-generator system using improved particle swarm optimization," *IEEE Trans. Ind. Electron.*, vol. 56, no. 5, pp. 1557–1577, May 2009.
[31] S. H. Ling, H. H. C. Iu, F. H. F. Leung, and K. Y. Chan, "Improved hybrid particle swarm optimized wavelet neural network for modeling the development of fluid dispensing for electronic packaging," *IEEE Trans. Ind. Electron.*, vol. 55, no. 9, pp. 3447–3460, Sep. 2008.
[32] A. Chatterjee, K. Pulasinghe, K. Watanabe, and K. Izumi, "A particle-swarm-optimized fuzzy-neural network for voice-controlled robot systems," *IEEE Trans. Ind. Electron.*, vol. 52, no. 6, pp. 1478–1489, Dec. 2005.
[33] I. N. Kassabalidis, M. A. El-Sharkawi, R. J. Marks, L. S. Moulin, and A. P. Alves da Silva, "Dynamic security border identification using enhanced particle swarm optimization," *IEEE Trans. Power Syst.*, vol. 17, no. 3, pp. 723–729, Aug. 2002.
[34] S. Naka, T. Genji, T. Yura, and Y. Fukuyama, "A hybrid particle swarm optimization for distribution state estimation," *IEEE Trans. Power Syst.*, vol. 18, no. 1, pp. 60–68, Feb. 2003.
[35] Z. L. Gaing, "A particle swarm optimization approach for optimum design of PID controller in AVR system," *IEEE Trans. Energy Convers.*, vol. 19, no. 2, pp. 384–391, Jun. 2004.
[36] H. Ishibuchi and T. Nakaskima, "Improving the performance of fuzzy classifier systems for pattern classification problems with continuous attributes," *IEEE Trans. Ind. Electron.*, vol. 46, no. 6, pp. 1057–1068, Dec. 1999.
[37] W. Y. Yang, W. Cao, T. S. Chung, and J. Morris, *Applied Numerical Methods Using MATLAB*. New York: Wiley, 2005, ch. 6.
[38] A. B. Arsoy, Y. Liu, P. F. Ribeiro, and F. Wang, "STATCOM-SMES," *IEEE Ind. Appl. Mag.*, vol. 9, no. 2, pp. 21–28, Mar./Apr. 2003.
[39] K. J. Astrom and B. Wittenmark, *Adaptive Control*. New York: Addison-Wesley, 1995.
[40] Y. Y. Hsu and K. L. Liou, "Design of self-tuning PID power system stabilizers for synchronous generators," *IEEE Trans. Energy Convers.*, vol. EC-2, no. 3, pp. 343–348, Sep. 1987.

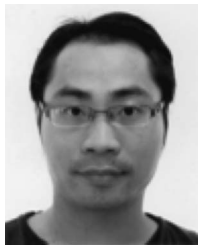

Chien-Hung Liu received the B.S. and M.S. degrees from the National Yunlin University of Science and Technology, Yunlin, Taiwan. He is currently working toward the Ph.D. degree at the National Taiwan University, Taipei, Taiwan.

His areas of research interest include power electronics, power quality, modern control, and power system analysis.

Yuan-Yih Hsu (S'82–M'82–SM'89) was born in Taiwan on June 19, 1955. He received the B.S., M.S., and Ph.D. degrees in electrical engineering from the National Taiwan University, Taipei, Taiwan.

Since 1977, he has been with the National Taiwan University, where he is currently a Professor. His current research interests include wind energy generation, reactive power compensation, and the application of power electronics to power systems.

Dr. Hsu was elected as one of the Ten Outstanding Young Engineers by the Chinese Institute of Engineers in 1989. He received the Distinguished Research Awards from the National Science Council in 1986 through 2007.